On the latitudinal extent of chorus emissions as observed by the Polar Plasma Wave Instrument

N. L. Bunch,[1] M. Spasojevic,[1] and Y. Y. Shprits[2,3]

Received 6 October 2010; revised 11 January 2011; accepted 20 January 2011; published 8 April 2011.

[1] The statistical distribution of chorus wave power in the off-equatorial region is evaluated using data from the Plasma Wave Instrument (PWI) Sweep Frequency Receiver (SFR) on board the Polar spacecraft. Maps of average wave power in the meridional plane divided into four local time sectors are presented. The geomagnetic dependence of wave power is examined, and substorm activity and enhanced solar wind speed result in distinctly different wave distributions. The maximum latitudinal extent of chorus as a function of latitude and L^* is estimated within the orbit constraints of the spacecraft, and on the basis of this the corresponding minimum resonant energy for first-order relativistic cyclotron resonance is calculated using a realistic magnetic field model.

Citation: Bunch, N. L., M. Spasojevic, and Y. Y. Shprits (2011), On the latitudinal extent of chorus emissions as observed by the Polar Plasma Wave Instrument, *J. Geophys. Res.*, *116*, A04204, doi:10.1029/2010JA016181.

1. Introduction

[2] The distribution of relativistic electrons that form the outer zone of Earth's radiation belts is extremely variable with the trapped flux observed to change by several orders of magnitude on time scales of a few hours to days [e.g., *Li et al.*, 2001; *Summers et al.*, 2007a, 2007b]. One process that is believed to play a major role in the dynamic evolution of the outer belt is cyclotron-resonant wave particle interactions involving whistler mode chorus emissions. Confoundingly, chorus interactions can result in the precipitative loss of electrons over a wide range of energies as well as the acceleration of seed electrons up to highly relativistic energies (>MeV) [e.g., *Horne and Thorne*, 1998; *Roth et al.*, 1999; *Meredith et al.*, 2003a, 2003b, 2003c; *Summers et al.*, 2004; *Horne et al.*, 2005a, 2005b; *Bortnik and Thorne*, 2007; *Shprits et al.*, 2008a, 2008b].

[3] In terms of losses of highly energetic electrons, chorus is believed to be the driver of relativistic microburst precipitation, which is characterized by short (<1 s), very intense, bursts of >1 MeV electron precipitation [*Blake et al.*, 1996]. Microbursts have been associated both temporally and spatially with individual chorus elements [*Lorentzen et al.*, 2001a], and further statistical analysis has shown that they occur predominantly across the morningside during disturbance intervals with a peak occurrence near 9 MLT [*O'Brien et al.*, 2003] similar to the distribution of chorus waves that extend to the off-equatorial region [*Tsurutani and Smith*, 1977].

[4] Microburst precipitation is a significant loss mechanism during storm intervals [e.g., *Lorentzen et al.*, 2001b; *O'Brien et al.*, 2004], and specifically *Thorne et al.* [2005] estimated effective electron lifetimes due to chorus to be on the order of a day or less and thus comparable to loss rates expected from other leading loss mechanisms such as plasmaspheric hiss and electromagnetic ion cyclotron waves [*Millan and Thorne*, 2007].

[5] *Thorne et al.* [2005] also showed that MeV electron scattering is most efficient during first-order cyclotron resonance with chorus in low-density regions (i.e., outside the plasmapause) at geomagnetic latitudes above 30°. Thus, further understanding and modeling of the global effects of chorus on relativistic losses requires knowledge of the distribution of wave power at higher magnetic latitudes. Several recent studies have produced global maps of chorus wave intensities [e.g., *Meredith et al.*, 2003c; *Pokhotelov et al.*, 2008; *Li et al.*, 2009], but statistics to date have been primarily limited to latitudes <25°.

[6] The Plasma Wave Instrument (PWI) [*Gurnett et al.*, 1995] on the Polar spacecraft (~18 h, ~2 × 9 R_E, ~90° inclination, North Pole apogee orbit) routinely observed chorus in the off-equatorial region. Recently, *Sigsbee et al.* [2010] derived chorus occurrence probabilities using the Polar PWI data set. Here we extend the work of *Sigsbee et al.* [2010] and use an independently derived database to answer the specific questions regarding the distribution of chorus wave power. Particularly, we quantify the maximum latitude at which significant wave power routinely exists and the geomagnetic dependance of wave power in the off-equatorial region. These derived quantities are a significant step forward in creating a global, dynamic model of chorus waves such as

[1]Space, Telecommunications, and Radioscience Laboratory, Department of Electrical Engineering, Stanford University, Stanford, California, USA.
[2]Institute of Geophysics and Planetary Physics, University of California, Los Angeles, California, USA.
[3]Department of Atmospheric Sciences, University of California, Los Angeles, California, USA.

0148-0227/11/2010JA016181

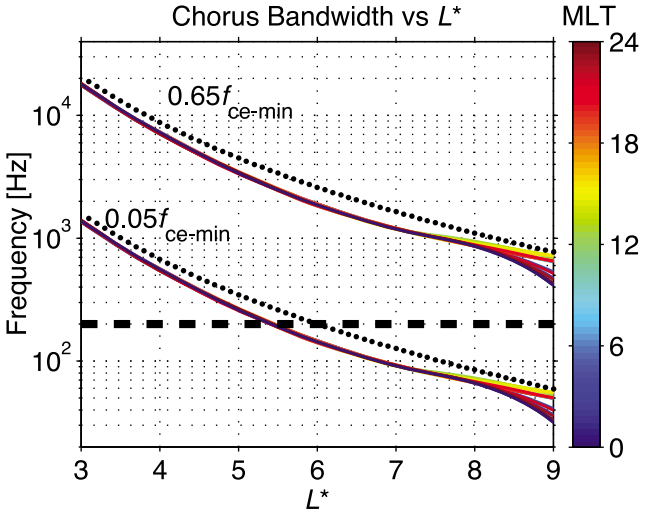

Figure 1. Typical frequency bounds for lower band chorus as a function of L^* for integer MLT values. Upper frequency limit corresponds to $0.65f_{ce}$ of the magnetic field line minima, while the lower limit is represented by $0.05f_{ce}$. Black dotted line represents the calculation using a dipole field model. Dashed black line indicates low-frequency cutoff due to noise considerations.

for inclusion in radiation belt models [e.g., *Horne et al.*, 2005b; *Fok et al.*, 2008; *Shprits et al.*, 2009].

2. Data Analysis

[7] The PWI includes a Sweep Frequency Receiver (SFR) that provides continuous (<1 min resolution), single-component electric (E) and magnetic (B) field measurements typically in a log-spaced frequency mode (26 Hz to 810 kHz). Chorus can be observed in SFR data on ascending and descending segments of the orbit outside the plasmapause and appears as a banded emission that approximately follows 0.5 of the estimated equatorial gyrofrequency in the dipolar polar region [*Santolik et al.*, 2009; *Omura et al.*, 2009] or possibly the minimum gyrofrequency [*Vaivads et al.*, 2007; *Menietti et al.*, 2009; *Spasojevic and Inan*, 2010] in the outer dayside field line bifurcation region [*Shabansky*, 1971].

[8] The spacecraft typically crosses the equator inside the plasmapause, and thus observations of chorus are primarily in the off-equatorial region of the northern hemisphere at $L > 4$.

[9] Chorus intervals were selected by visual inspection of full resolution SFR spectrograms of E and B power spectral density. The location of the spacecraft with respect to the plasmapause was inferred from the upper hybrid resonance band [*Mosier et al.*, 1973; *Sigsbee et al.*, 2008, 2010] as well as the presence of plasmaspheric hiss [*Dunckel and Helliwell*, 1969; *Russell et al.*, 1969; *Thorne et al.*, 1973]. Only chorus exclusively outside the plasmapause was selected. Many examples of discrete or chorus-like waves inside the plasmasphere are observed, but analysis of these emissions is beyond the scope of this investigation. Time periods of cross talk, interference, and high noise levels, such as those caused by eclipse or interference from the Electric Field Instrument, were also excluded. In order to ensure that the selected emissions are electromagnetic in nature, additional filtering by the output of the SFR onboard correlator was employed [cf. *Mellott et al.*, 1986; *Gurnett et al.*, 1995]. A threshold correlation value between the E and B channels of 0.84 was selected (a natural break at high correlation), where correlation is given on a scale between 0 and 1, and correlation between a waveform and itself equals 1. Thus, time periods where exclusively electric or magnetic field data were taken were also excluded.

[10] Figure 1 shows the nominal frequency range of lower band chorus observable by Polar as a function of L^* and MLT, using a *Tsyganenko* [1989] magnetic field model with $Kp = 2$.

[11] Following *Horne et al.* [2005b], the upper and lower frequency bounds correspond to 0.65 and 0.05 times the minimum gyrofrequency of the field line. As originally characterized by *Burtis and Helliwell* [1976], we assume wave power to be approximately Gaussian about its wave amplitude peak and center frequency of 0.35 times the minimum gyrofrequency, consistent with the way chorus is typically characterized as an input to radiation belt models [e.g., *Horne et al.*, 2005b; *Summers*, 2005; *Shprits et al.*, 2006]. Because of the high noise floor of the SFR at frequencies below 200 Hz, indicated by the black dashed line in Figure 1, only chorus above 200 Hz has been considered in this study (also employed by *Sigsbee et al.* [2008]). Although the very lowest frequency components of chorus are undetectable by the Polar PWI for $L^* > 5$, assuming chorus wave power is approximately spread across its center frequency, the frequency range observable by Polar provides opportunity to obtain representative chorus power spectral densities for the full orbital path. For instance, more than 50% of the chorus frequency band is detectable by Polar even at $L^* \approx 9$, where the greatest fraction of chorus lies below 200 Hz.

[12] Previous statistical investigations of chorus wave intensity have primarily focused on presenting average magnetic wave power integrated across the approximated chorus frequency band averaged over all time (i.e., including times when chorus was not observed) [e.g., *Meredith et al.*, 2003b, 2003c; *Li et al.*, 2009] since this is a first-order input to global diffusion models [e.g., *Shprits et al.*, 2009]. Several studies have calculated B field values using E field measurements and a cold plasma whistler dispersion relation [e.g., *Meredith et al.*, 2003a, 2003b, 2003c]. These types of analyses may underestimate the wave power of chorus in the outer magnetosphere where distorted magnetospheric configurations cause chorus to lie outside the expected band, and over estimate contributions in regions conducive to noise, electrostatic waves, magnetosonic waves and hiss. For these reasons we have employed use of visual inspection and the onboard correlator to isolate only electromagnetic chorus power spectral densities as representative of chorus intensity for all regions of orbital coverage. Moreover, the combination of typical wave intensity considered here and occurrence rates examined by *Sigsbee et al.* [2010] provide a more complete picture of chorus characteristics within the provided sampling space. Extrapolation of power spectral densities to integrated wave power could be performed, considering the above caveats, but it is beyond the scope of the current study and will be addressed in future analysis.

[13] In the frequency range where chorus is typically observed (200 Hz to 12.5 kHz), the SFR obtained field

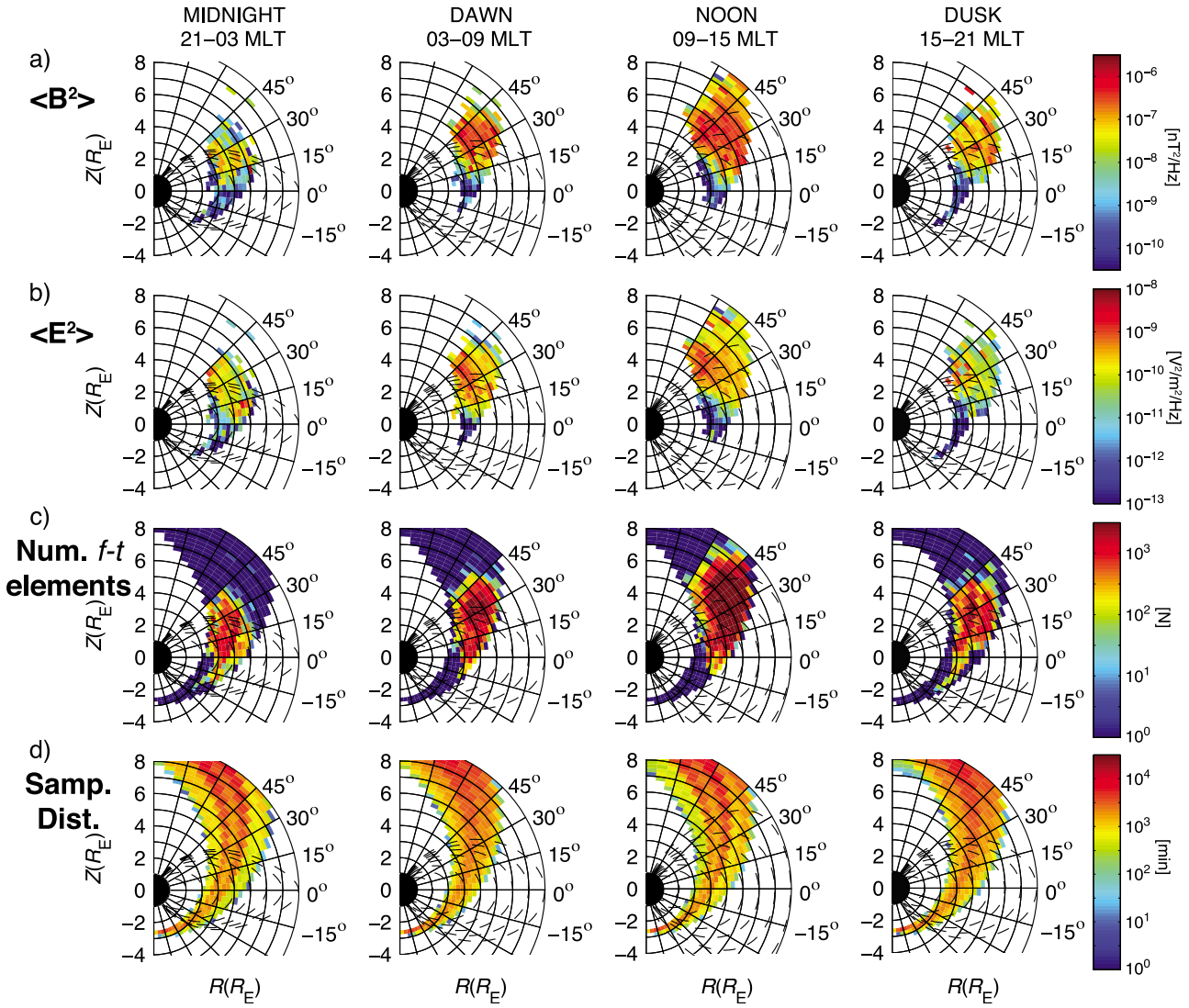

Figure 2. Mean chorus (a) B and (b) E power spectral density binned by 5° in magnetic latitude (λ) and 0.25 R_E in radial distance (R) in the indicated local time sector. (c) The total number of f-t elements used in each calculated mean in Figures 2a and 2b. (d) Spatial sampling distribution by Polar showing number of minutes in each bin. Each plot displays Z_{SM} on the vertical axis and radial distance in the X-Y_{SM} plane on the horizontal axis. Field lines are from the *Tsyganenko* [1989] magnetic field model with Kp = 2.

measurements in two bands (200–1600 Hz and 1.6–12.5 kHz) each with 32 log spaced frequencies sampled at a cadence of 16.5 s and 8.2 s per sweep, respectively, [*Gurnett et al.*, 1995]. Chorus was resolved by the SFR on 459 out of 1388 half orbits between 25 March 1996 and 16 September 1997 for a total of 584,811 frequency-time (f-t) spectral density elements for use in statistical analysis. For each f-t element, the L^* value [*Roederer*, 1970] was calculated using the ONERA-DESP library and the *Tsyganenko* [1989] magnetic field model and the concomitant value of the Kp index.

3. Variation in Radial Distance, Magnetic Latitude, and Magnetic Local Time

[14] Because of the polar orbit of the spacecraft, the PWI derived maps of chorus wave power are best represented in a meridional plane view and separated by magnetic local time (MLT) sector. Figure 2 shows the statistical distribution of chorus mean B and E power spectral density, the total number of f-t power spectral density elements used in calculating that mean, as well as the spatial sampling distribution of Polar for each time sector. In Figure 2c, the total area of the colored swaths indicate the limits of the orbital coverage. Dark blue regions indicate where no chorus was observed. Figure 2d shows the spatial region sampled by Polar, indicating the number of minutes spent in each (R,λ) bin.

[15] Note that while Figure 2d is indicative of the opportunity to observe waves, Figure 2c not only provides statistical confidence in average wave power values shown in Figures 2a–2b, the distribution of f-t elements in the R-λ plane is additionally symptomatic of the probability of observing waves in a given region as previously discussed by *Sigsbee et al.* [2010].

[16] There is a striking day/night asymmetry both in the wave distribution and power. In the midnight sector, waves extend out to $R \approx 6\ R_E$ while at noon they extend out to the limits of orbital coverage ($R \approx 9\ R_E$). The dawn and noon sectors show the highest wave power with the region of observed waves ranging up to $\lambda \approx 45°$ and 60°, respectively. The region in the R-λ plane occupied by waves in the dusk sector is spatially similar to that at dawn although power spectral densities are more comparable to observations around midnight. Consistent with the findings of *Santolik et al.* [2005], power spectral densities appear to decrease inside of the field line trace crossing the equator at 6 R_E. Note, however, that since the frequency and bandwidth of chorus scale as $\sim L^{-3}$, high spectral densities at large L may or may not imply greater total wave power due to the narrower bandwidth.

[17] One may note that the outer dayside region, which shows the highest density of collected f-t elements, also appears to exhibit the highest average power spectral density. It not surprising that, since they are the most conducive to wave growth, regions of highest observation density might also have the highest typical wave powers. This apparent correlation, however, appears confined to the high-latitude dayside regions. Regions below ~30° (approximately $5 < L^* < 8$) also display high observation density but show decreasing power spectral density since these observations are confined to lower L shells where chorus has larger bandwidths. Additionally, the midnight sector also shows significant statistics but considerably lower spectral densities. This result highlights the importance of determining typical chorus wave power and occurrence rates separately, since both impact the ultimate chorus wave power distribution as a function of space and time.

[18] A major goal of the current study is to quantify the latitudinal extent of intense chorus waves as a function of local time. Figure 3a shows the mean B power spectral density as a function of λ and MLT for all values of L^*. Figure 3b shows the number of f-t elements used to calculate each mean. Again, there is wave power at significantly higher latitudes in the noon sector, and a periodic function fit by least squares has been applied to the plot to emphasize this trend. This trend continues when the data is further divided by L^* (not shown). Depicting a similar trend, Figure 3c shows the highest magnetic latitude at which chorus was observed for each half orbit as a function of MLT and L^*, suggesting that observation of chorus ranging up to such high latitudes and L^*, particularly on the dayside, is not only possible but, in fact, typical. Note, however, that because of orbital constraints, observations at lower values of L^* are limited to lower latitudes. Thus, Figure 3d shows the estimated latitudinal extent of the waves as a function of L^* where the dashed lines indicate that the waves extend up to the latitudinal limit of the spacecraft coverage. Using these curves, the minimum (parallel) resonant energy ($\mathcal{E}_{\|}$) is calculated for first-order relativistic electron-cyclotron reso-

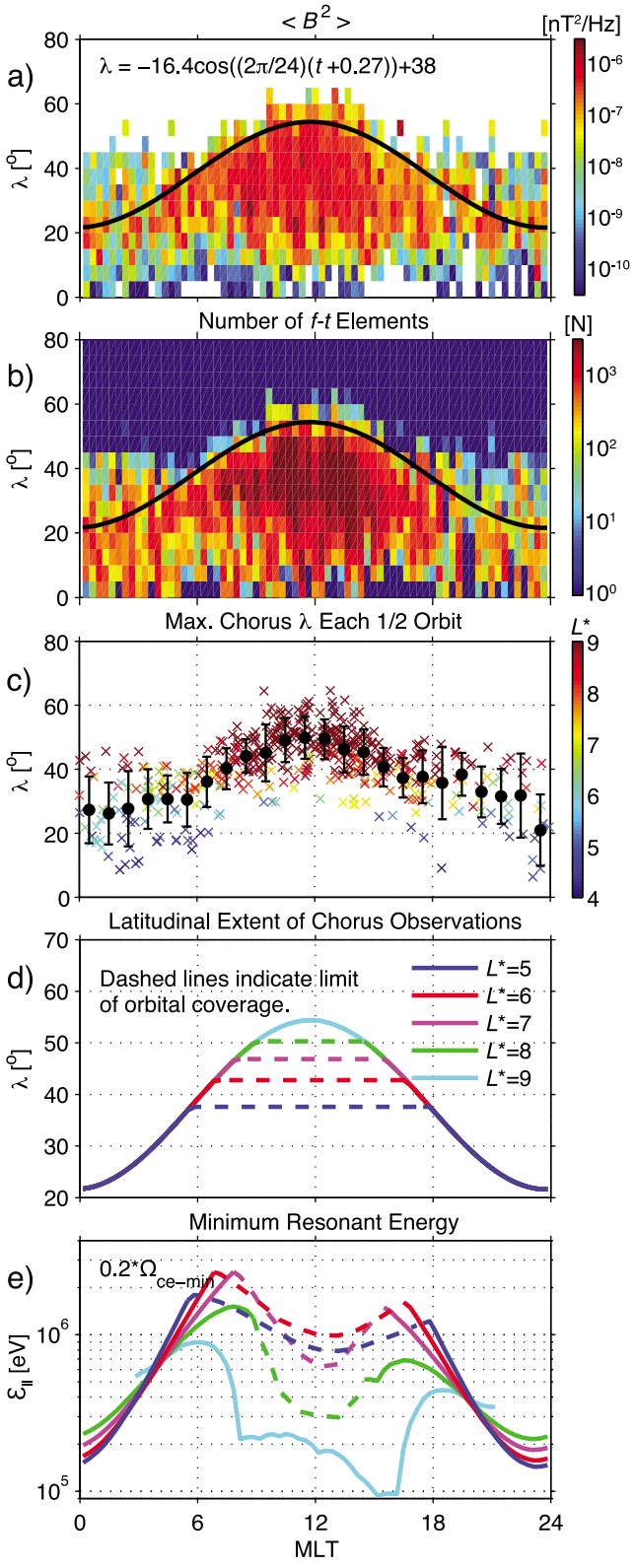

Figure 3. (a) Mean B power spectral density as a function of λ and MLT for all values of L^*. (b) Number of f-t elements used in each calculated mean in Figure 3a. (c) Maximum magnetic latitude at which chorus was observed for each half orbit for which waves were present. Black dots and error bars indicate mean and standard deviation values for each hour of MLT. (d) Estimated extent in λ of chorus as a function of L^*. (e) Minimum resonant energy for cyclotron resonance at the λ from Figure 3d as a function of L^*.

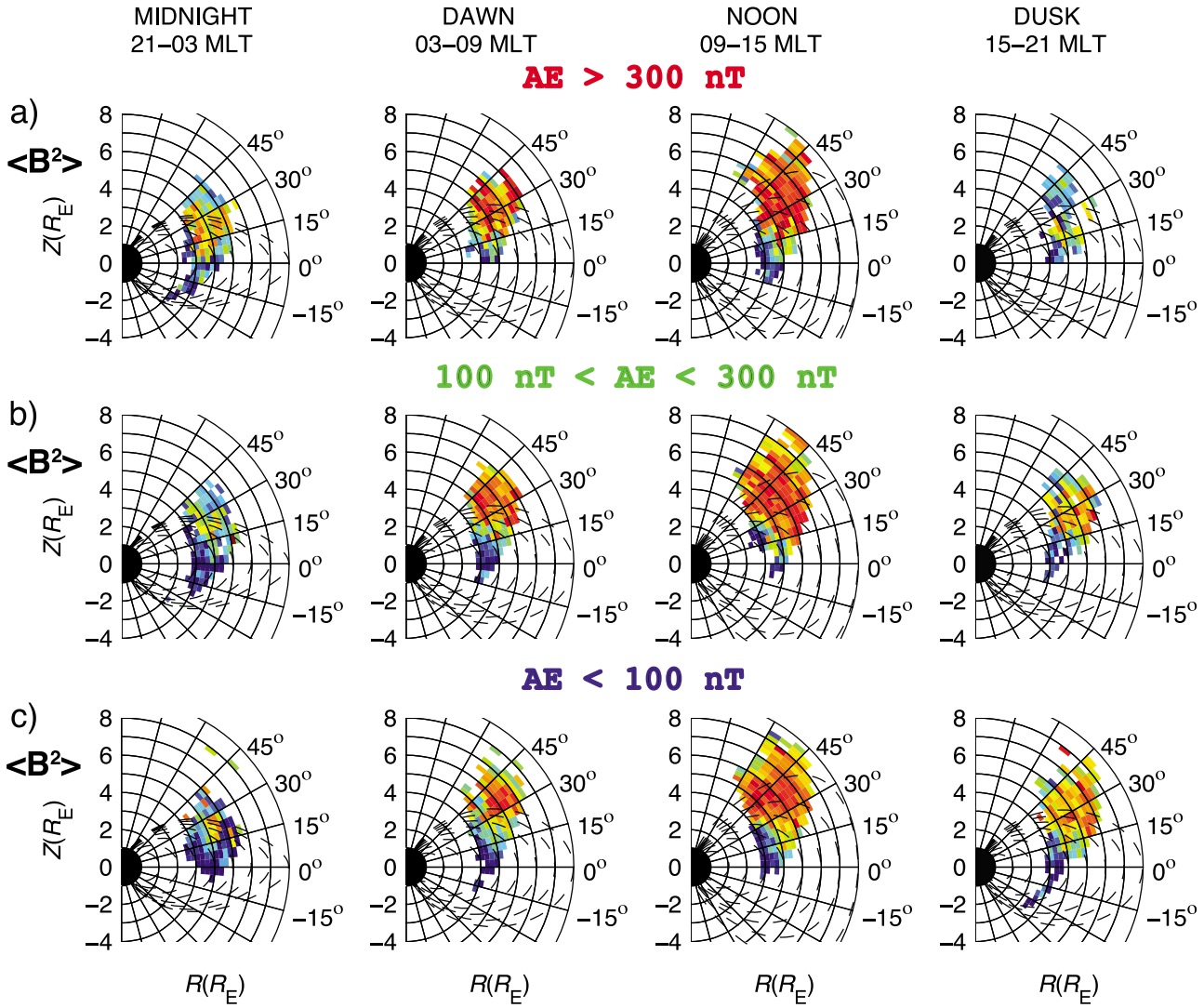

Figure 4. Substorm dependence of chorus mean B power spectral density for local time sectors indicated. Color scale is the same as Figure 2a.

nance (Figure 3e). The local B field strength is taken from the *Tsyganenko* [1989] field model with Kp = 2, and the waves are assumed to be at 0.2 of the minimum gyrofrequency along the field line. The cold plasma density is from the *Sheeley et al.* [2001] equatorial trough model and is scaled latitudinally as in work by *Denton et al.* [2004]. The wave vector is determined by the cold whistler mode dispersion relation assuming parallel propagation for determination of the minimum energy. The calculation of minimum resonant energy is conventionally used as a rough estimate because of the assumption of only parallel propagation. One may note however that wave normals of lower band chorus in the off equatorial region, where its wave power typically dominates [*Meredith et al.*, 2001], are observed over a broad range of angles and are often observed close to parallel (<20°) [*Haque et al.*, 2010; *Muto et al.*, 1987; *Burton and Holzer*, 1974].

[19] In the midnight sector, $\mathcal{E}_{||}$ increases with increasing L^*. This is the result of field line stretching which causes the field strength to rapidly increase with increasing latitude at higher L^* values [e.g., *Orlova and Shprits*, 2010]. Moving around the dawn and dusk flanks, this trend reverses as the field becomes more dipolar such that $\mathcal{E}_{||}$ decreases with increasing L^*. In the noon sector, $\mathcal{E}_{||}$ decreases across all L^* values as a result of dayside compression of the field. Again we note that in the noon sector, the observations are limited by the orbit coverage of the spacecraft (dashed lines), and $\mathcal{E}_{||}$ could extend to higher values. Additionally, there is a dawn-dusk asymmetry in $\mathcal{E}_{||}$ due to the increasing cold plasma density across the dayside. The most favorable region for interaction of chorus with MeV electrons is 4–10 MLT for $L^* < 7$.

4. Variation With Geomagnetic Activity

[20] Next, we explore the variation of chorus wave power with geomagnetic activity. Figure 4 shows mean B power spectral density for three levels of the auroral electrojet (AE) index. For AE > 300 nT, <300 but >100 nT, and <100 nT, a total of 130,574, 205,423, and 248,814 f-t elements were used to compute the displayed average wave powers,

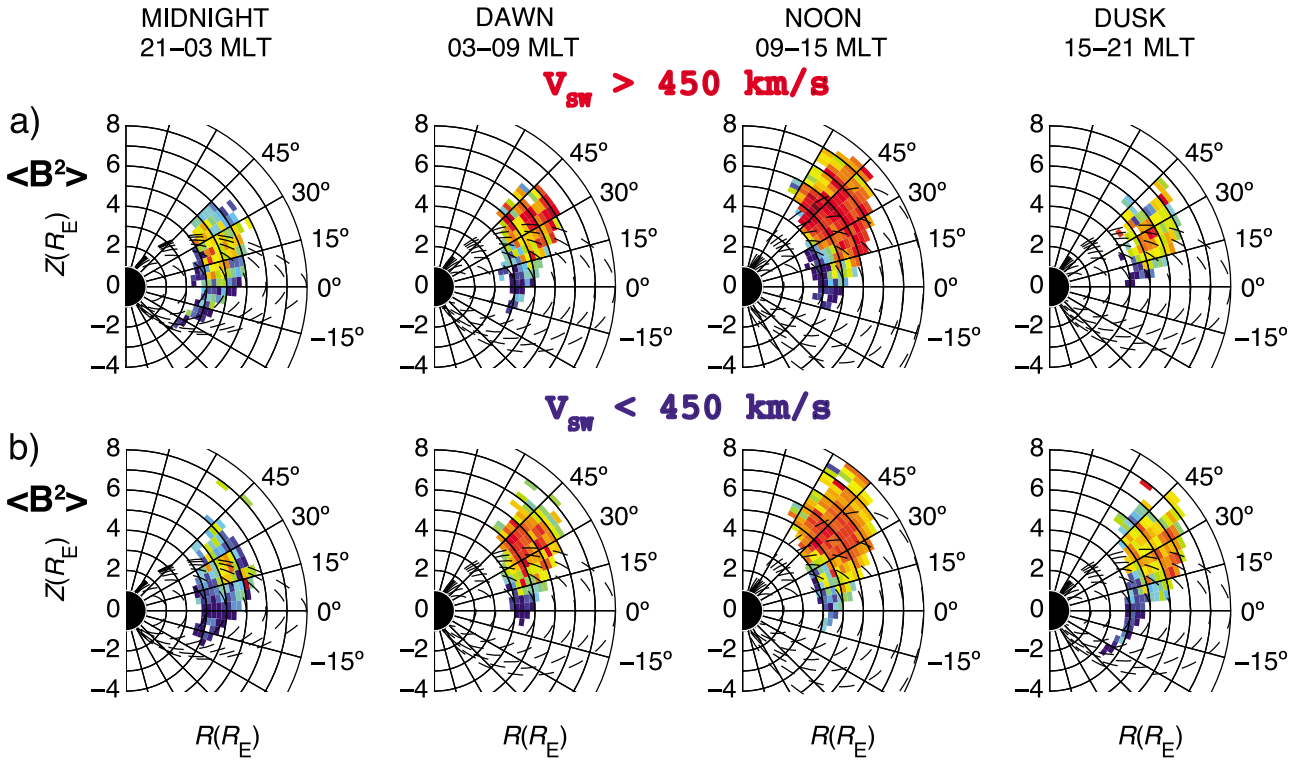

Figure 5. Solar wind speed dependence of chorus mean B power spectral density for local time sectors indicated. Color scale is the same as Figure 2a.

respectively. These represent 22.3, 35.1, and 42.6% of the total number of f-t elements used in this study. Additionally, the AE index was >300, <300 and >100, and <100 nT for 16.7, 32.1, and 51.2% of the time interval used in this study. The increase in mean wave power for high geomagnetic activity (AE > 300 nT) as compared to quiet times (AE < 100 nT) for the region of optimal statistics (4 $R_E < R < 8$ R_E, $15° < \lambda < 45°$) shows a change in intensity for the midnight, dawn, noon, and dusk sectors of +27%, +88%, +60%, and −71% respectively.

[21] *Sigsbee et al.* [2010] showed that the probability of occurrence of chorus increases by a factor of ~2 for solar wind speeds (V_{SW}) above 450 km/s as compared to below 450 km/s. Figure 5, analogous to Figure 4, shows mean B power spectral density for solar wind speed greater and less than 450 km/s. For V_{SW} > 450 km/s and <450 km/s, a total of 215,665 and 369,146 f-t elements were used to compute the displayed average wave powers, respectively. These represent 36.9, and 63.1% of the total number of f-t elements used in this study. Additionally, the solar wind velocity was >450 and <450 km/s for 20.6%, and 79.4% of the time interval used in this study. We find chorus wave power also shows variation for V_{SW} above 450 km/s compared to below 450 km/s, with midnight, dawn, noon, and dusk, employing the same region of optimal statistics, varying by −23%, −2.7%, +84%, and +40%.

5. Summary and Discussion

[22] Statistical analysis of Polar PWI data has contributed to our understanding of the global distribution of chorus wave power, particularly in the off-equatorial region and its implications for scattering relativistic electrons. Waves in the noon sector are observed with high wave power over a large spatial region. Estimates of the extent in λ of the waves are limited by the spacecraft coverage, and chorus extends at least up to $\lambda \approx 30°$ at $L^* = 5$ and $\lambda \approx 55°$ at $L^* = 9$. Average wave power in this sector increases by more than 80% during both enhanced substorm activity (from AE < 100 to >300) and during enhanced solar wind speed (from V_{SW} < 450 to >450). It has previously been shown for the near-equatorial region that the dayside outer magnetosphere is particularly conducive to wave growth over a wide range of geomagnetic conditions [e.g., *Koons and Roeder*, 1990; *Santolik et al.*, 2005; *Li et al.*, 2009], and we show here that this result extends to significantly higher latitudes. Substorms increase the flux of source electrons while enhanced solar wind velocity increases the quiescent anisotropy (through enhanced drift shell splitting). *Spasojevic and Inan* [2010] pointed out that solar wind compression of the dayside also creates extended regions of B field homogeneity along the field line, which is a favorable condition for nonlinear wave growth [*Nunn*, 1974; *Omura et al.*, 1991]. This effect may further contribute to the high latitudinal extent of the noon sector waves reported here.

[23] Near dawn, the average power of the waves is similar to that at noon, but the extent of the waves in λ is somewhat reduced. Increased substorm activity in this sector leads to increased wave power, but enhanced V_{SW} appears to have little effect perhaps since the field geometry in that region is less solar wind dependent.

[24] In the midnight sector, wave power is confined within a significantly smaller spatial region than at noon, approximately inside of $L^* < 7$ and $\lambda < 25°$. Near midnight increased substorm activity shows an increase in the average wave power, but enhanced V_{SW} reveals a reduction by a similar percentage. This may be complimentary to the effect at noon since at midnight, enhanced V_{SW} elongates the field lines causing the B field to increase rapidly with latitude. Thus, nonlinear wave growth is achieved only over a narrow region in λ about the equator.

[25] Although chorus is observed the least often in the dusk sector [*Sigsbee et al.*, 2010], an interesting effect is found wherein, unlike all other sectors, average wave power decreases with increasing substorm activity. This could be the result of the opening of electron drift paths such that the source electrons are lost to the magnetopause before drifting to dusk or the formation of a plasmaspheric plume limiting wave growth or causing wave damping during storm time substorms.

[26] These results illustrate the likelihood that both increased substorm activity and solar wind speed can contribute, both individually and in concert, to the generation of intense chorus waves in the off equatorial outer magnetosphere. Originally proposed by *Tsurutani and Smith* [1977], these observations appear consistent with chorus driven by increased anisotropy on the dayside due mainly to magnetospheric compression, while reduced anisotropy occurs on the night side because of elongation. It is also consistent with suggestion by *Spasojevic and Inan* [2010] that increased solar wind speeds lead to latitudinally enlarged (reduced) wave growth or minimum B regions on the dayside (nightside). For the case of increased AE, a different pattern is observed, where midnight, dawn and noon see significant increases in wave intensity, while the dusk sector reduces by over 70%. This suggests a different chorus driver, enhanced source population during substorms, the foremost explanation for chorus waves, where the midnight, dawn, and noon sectors see significant wave growth, but because of the path of enhanced convection and the extended duskside plume, waves are likely not to grow or to be damped for the dusk sector. For substorms where solar wind speed is also increased, a not uncommon occurrence, regions of magnetic field homogeneity increase [*Spasojevic and Inan*, 2010] and drift paths shift away from the equator to higher latitudes which results in drift shell splitting, or "Shabansky" orbital paths [e.g., *Shabansky*, 1971] in the outer dayside magnetosphere. This scenario provides a very conducive environment for wave generation at high latitudes across the dayside outer zone. Thus, much as originally proposed by *Tsurutani and Smith* [1977], off equatorial chorus in the outer magnetosphere may represent a somewhat separate chorus population to that observed in the inner magnetosphere near the equator, and may typically be driven by a more combined influence of both magnetospheric compression and substorm activity.

[27] The estimated extent in λ of the waves was used to bound the parallel resonant electron energy as a function of MLT and L^* using a realistic B field model. The most favorable region for interaction of chorus with MeV electrons is 4–10 MLT for $L^* < 7$, and we note that the observations here are generally limited to $L^* > 5$. This is the result of the high latitudinal extent of the waves combined with the low plasma density and the more dipolar field geometry in the late morning sector and is consistent with the current picture for MeV microburst precipitation [*O'Brien et al.*, 2003]. Note however that chorus waves may interact at higher energies than shown in Figure 3e if waves persist above dashed lines shown in Figure 3d and oblique wave normals are considered [cf. *Orlova and Shprits*, 2010].

[28] The Polar PWI SFR records provide a means of evaluating the distribution of average chorus wave power in the off-equatorial region and its geomagnetic dependence. The latitudinal extent of chorus, as quantified here, determines the highest-energy electrons that can be efficiently scattered by the waves. The above parameters are needed to evaluate energetic electron loss rates such as through the use of global quasi-linear diffusion models [e.g., *Shprits et al.*, 2009]. As a final note, however, we recognize that chorus is a discrete emission composed of individual wave elements, and full quantification of the role of chorus requires understanding the complex nonlinear interactions that may lead to more rapid growth and pitch angle and energy scattering than modeled by linear wave growth and scattering by quasi-linear theory [e.g., *Bortnik et al.*, 2008; *Furuya et al.*, 2008; *Omura et al.*, 2008; *Tsurutani et al.*, 2009].

[29] **Acknowledgments.** The OMNI data were obtained from the GSFC/SPDF OMNIWeb interface at http://omniweb.gsfc.nasa.gov. We thank D. Boscher, S. Bourdarie, P. O'Brien, and T. Guild for providing the ONERA-DESP library V4.2, Toulouse-France, 2004–2008, available at http://craterre.onecert.fr/support/user_guide.html. The *AE* and *Kp* indices were provided by the Kyoto World Data Center for Geomagnetism. This research was supported by the NASA Living With a Star Heliophysics Postdoctoral Fellowship Program, administered by the UCAR Visiting Scientist Programs, as well as NASA grant NNX09AF51G.

[30] Robert Lysak thanks the reviewers for their assistance in evaluating this paper.

References

Blake, J. B., M. D. Looper, D. N. Baker, R. Nakamura, B. Klecker, and D. Hovestadt (1996), New high temporal and spatial resolution measurements by SAMPEX of the precipitation of relativistic electrons, *Adv. Space Res*, *18*(8), 171–186, doi:10.1016/0273-1177(95)00969-8.

Bortnik, J., and R. M. Thorne (2007), The dual role of ELF/VLF chorus waves in the acceleration and precipitation of radiation belt electrons, *J. Atmos. Sol. Terr. Phys.*, *69*, 377–386, doi:10.1016/j.jastp.2006.05.030.

Bortnik, J., R. M. Thorne, and U. S. Inan (2008), Nonlinear interaction of energetic electrons with large amplitude chorus, *Geophys. Res. Lett.*, *35*, L21102, doi:10.1029/2008GL035500.

Burtis, W. J., and R. A. Helliwell (1976), Magnetospheric chorus: Occurrence patterns and normalized frequency, *Planet. Space Sci.*, *24*, 1007–1024, doi:10.1016/0032-0633(76)90119-7.

Burton, R. K., and R. E. Holzer (1974), The origin and propagation of chorus in the outer magnetosphere, *J. Geophys. Res.*, *79*, 1014–1023, doi:10.1029/JA079i007p01014.

Denton, R. E., J. D. Menietti, J. Goldstein, S. L. Young, and R. R. Anderson (2004), Electron density in the magnetosphere, *J. Geophys. Res.*, *109*, A09215, doi:10.1029/2003JA010245.

Dunckel, N., and R. A. Helliwell (1969), Whistler mode emissions on the OGO 1 satellite, *J. Geophys. Res.*, *74*, 6371–6385, doi:10.1029/JA074i026p06371.

Fok, M. C., R. B. Horne, N. P. Meredith, and S. A. Glauert (2008), Radiation belt environment model: Application to space weather nowcasting, *J. Geophys. Res.*, *113*, A03S08, doi:10.1029/2007JA012558.

Furuya, N., Y. Omura, and D. Summers (2008), Relativistic turning acceleration of radiation belt electrons by whistler mode chorus, *J. Geophys. Res.*, *113*, A04224, doi:10.1029/2007JA012478.

Gurnett, D. A., A. M. Persoon, R. F. Randall, D. L. Odem, S. L. Remington, T. F. Averkamp, M. M. Debower, G. B. Hospodarsky, R. L. Huff, and D. L. Kirchner (1995), The Polar Plasma Wave Instrument, *Space Sci. Rev.*, *71*(1–4), 597–622, doi:10.1007/BF00751343.

Haque, N., M. Spasojevic, O. Santolik, and U. S. Inan (2010), Wave normal angles of magnetospheric chorus emissions observed on the Polar spacecraft, *J. Geophys. Res.*, *115*, A00F07, doi:10.1029/2009JA014717.

Horne, R. B., and R. M. Thorne (1998), Potential waves for relativistic electron scattering and stochastic acceleration during magnetic storms, *Geophys. Res. Lett.*, *25*, 3011–3014, doi:10.1029/98GL01002.

Horne, R. B., et al. (2005a), Wave acceleration of electrons in the Van Allen radiation belts, *Nature*, *437*, 227–230, doi:10.1038/nature03939.

Horne, R. B., R. M. Thorne, S. A. Glauert, J. M. Albert, N. P. Meredith, and R. R. Anderson (2005b), Timescale for radiation belt electron acceleration by whistler mode chorus waves, *J. Geophys. Res.*, *110*, A03225, doi:10.1029/2004JA010811.

Koons, H. C., and J. L. Roeder (1990), A survey of equatorial magnetospheric wave activity between 5 and 8 R_E, *Planet. Space Sci.*, *38*, 1335–1341, doi:10.1016/0032-0633(90)90136-E.

Li, W., R. M. Thorne, V. Angelopoulos, J. Bortnik, C. M. Cully, B. Ni, O. LeContel, A. Roux, U. Auster, and W. Magnes (2009), Global distribution of whistler-mode chorus waves observed on the THEMIS spacecraft, *Geophys. Res. Lett.*, *36*, L09104, doi:10.1029/2009GL037595.

Li, X., D. N. Baker, S. G. Kanekal, M. Looper, and M. Temerin (2001), Long term measurements of radiation belts by SAMPEX and their variations, *Geophys. Res. Lett.*, *28*, 3827–3830, doi:10.1029/2001GL013586.

Lorentzen, K. R., J. B. Blake, U. S. Inan, and J. Bortnik (2001a), Observations of relativistic electron microbursts in association with VLF chorus, *J. Geophys. Res.*, *106*, 6017–6027, doi:10.1029/2000JA003018.

Lorentzen, K. R., M. D. Looper, and J. B. Blake (2001b), Relativistic electron microbursts during the GEM storms, *Geophys. Res. Lett.*, *28*, 2573–2576, doi:10.1029/2001GL012926.

Mellott, M. M., R. L. Huff, and D. A. Gurnett (1986), DE 1 observations of harmonic auroral kilometric radiation, *J. Geophys. Res.*, *91*, 13,732–13,738.

Menietti, J. D., O. Santolik, and P. C. Abaci (2009), Chorus observations by the Polar spacecraft near the mid-altitude cusp, *Planet. Space Sci.*, *57*, 1412–1418, doi:10.1016/j.pss.2009.07.003.

Meredith, N. P., R. B. Horne, and R. R. Anderson (2001), Substorm dependence of chorus amplitudes: Implications for the acceleration of electrons to relativistic energies, *J. Geophys. Res.*, *106*, 13,165–13,178.

Meredith, N. P., R. B. Horne, D. Summers, R. M. Thorne, R. H. A. Iles, D. Heynderickx, and R. R. Anderson (2003a), Evidence for acceleration of outer zone electrons to relativistic energies by whistler mode chorus, *Ann. Geophys.*, *20*, 967–979.

Meredith, N. P., M. Cain, R. B. Horne, R. M. Thorne, D. Summers, and R. R. Anderson (2003b), Evidence for chorus-driven electron acceleration to relativistic energies from a survey of geomagnetically disturbed periods, *J. Geophys. Res.*, *108*(A6), 1248, doi:10.1029/2002JA009764.

Meredith, N. P., R. B. Horne, R. M. Thorne, and R. R. Anderson (2003c), Favored regions for chorus-driven electron acceleration to relativistic energies in the Earth's outer radiation belt, *Geophys. Res. Lett.*, *30*(16), 1871, doi:10.1029/2003GL017698.

Millan, R. M., and R. M. Thorne (2007), Review of radiation belt relativistic electron losses, *J. Atmos. Sol. Terr. Phys.*, *69*, 362–377, doi:10.1016/j.jastp.2006.06.019.

Mosier, S., M. Kaiser, and L. Brown (1973), Observations of noise bands associated with the upper hybrid resonance by the Imp 6 radio astronomy experiment, *J. Geophys. Res.*, *78*, 1673–1679, doi:10.1029/JA078i010p01673.

Muto, H., M. Hayakawa, M. Parrot, and F. Lefeuvre (1987), Direction finding of half-gyrofrequency VLF emissions in the off-equatorial region of the magnetosphere and their generation and propagation, *J. Geophys. Res.*, *92*, 7538–7550, doi:10.1029/JA092iA07p07538.

Nunn, D. (1974), A self-consistent theory of triggered VLF emissions, *Planet. Space Sci.*, *22*, 349–378, doi:10.1016/0032-0633(74)90070-1.

O'Brien, T. P., K. R. Lorentzen, I. R. Mann, N. P. Meredith, J. B. Blake, J. F. Fennell, M. D. Looper, D. K. Milling, and R. R. Anderson (2003), Energization of relativistic electrons in the presence of ULF power and MeV microbursts: Evidence for dual ULF and VLF acceleration, *J. Geophys. Res.*, *108*(A8), 1329, doi:10.1029/2002JA009784.

O'Brien, T. P., M. D. Looper, and J. B. Blake (2004), Quantification of relativistic electron microburst losses during the GEM storms, *Geophys. Res. Lett.*, *31*, L04802, doi:10.1029/2003GL018621.

Omura, Y., D. Nunn, H. Matsumoto, and M. J. Rycroft (1991), A review of observational, theoretical and numerical studies of VLF triggered emissions, *J. Atmos. Sol. Terr. Phys.*, *53*, 351–368, doi:10.1016/0021-9169(91)90031-2.

Omura, Y., Y. Katoh, and D. Summers (2008), Theory and simulation of the generation of whistler-mode chorus, *J. Geophys. Res.*, *113*, A04223, doi:10.1029/2007JA012622.

Omura, Y., M. Hikishima, Y. Katoh, D. Summers, and S. Yagitani (2009), Nonlinear mechanisms of lower-band and upper-band VLF chorus emissions in the magnetosphere, *J. Geophys. Res.*, *114*, A07217, doi:10.1029/2009JA014206.

Orlova, K. G., and Y. Y. Shprits (2010), Dependence of pitch-angle scattering rates and loss timescales on the magnetic field model, *Geophys. Res. Lett.*, *37*, L05105, doi:10.1029/2009GL041639.

Pokhotelov, D., F. Lefeuvre, R. B. Horne, and N. Cornilleau-Wehrlin (2008), Survey of ELF-VLF plasma waves in outer radiation belt observed by Cluster STAFF-SA experiment, *Ann. Geophys.*, *26*, 3269–3277, doi:10.5194/angeo-26-3269-2008.

Roederer, J. G. (1970), *Dynamics of Geomagnetically Trapped Radiation, Physics and Chemistry in Space*, vol. 2, Springer, New York.

Roth, I., M. A. Temerin, and M. K. Hudson (1999), Resonant enhancement of relativistic electron fluxes during geomagnetically active periods, *Ann. Geophys.*, *17*, 631–638, doi:10.1007/s00585-999-0631-2.

Russell, C. T., R. E. Holzer, and E. J. Smith (1969), OGO 3 observations of ELF noise in the magnetosphere: 1. Spatial extent and frequency of occurrence, *J. Geophys. Res.*, *74*, 755–777, doi:10.1029/JA074i003p00755.

Santolik, O., E. Macusova, K. H. Yearby, N. Cornilleau-Wehrlin, and H. S. K. Alleyne (2005), Radial variation of whistler-mode chorus: First results from the STAFF/DWP instrument onboard the Double Star TC 1 spacecraft, *Ann. Geophys.*, *23*, 2937–2942, doi:10.5194/angeo-23-2937-2005.

Santolik, O., D. A. Gurnett, J. S. Pickett, J. Chum, and N. Cornilleau-Wehrlin (2009), Oblique propagation of whistler mode waves in the chorus source region, *J. Geophys. Res.*, *114*, A00F03, doi:10.1029/2009JA014586.

Shabansky, V. P. (1971), Some processes in the magnetosphere, *Space Sci. Rev.*, *12*, 299–418, doi:10.1007/BF00165511.

Sheeley, B., M. Moldwin, H. Rassoul, and R. Anderson (2001), An empirical plasmasphere and trough density model: CRRES observations, *J. Geophys. Res.*, *106*, 25,631–25,641, doi:10.1029/2000JA000286.

Shprits, Y. Y., R. M. Thorne, R. B. Horne, and D. Summers (2006), Bounce-averaged diffusion coefficients for field-aligned chorus waves, *J. Geophys. Res.*, *111*, A10225, doi:10.1029/2006JA011725.

Shprits, Y. Y., S. R. Elkington, N. P. Meredith, and D. A. Subbotin (2008a), Review of modeling of losses and sources of relativistic electrons in the outer radiation belt: I. Radial transport, *J. Atmos. Sol. Terr. Phys.*, *70*, 1679–1693, doi:10.1016/j.jastp.2008.06.008.

Shprits, Y. Y., D. A. Subbotin, N. P. Meredith, and S. R. Elkington (2008b), Review of modeling of losses and sources of relativistic electrons in the outer radiation belt: II. Local acceleration and loss, *J. Atmos. Sol. Terr. Phys.*, *70*, 1694–1713, doi:10.1016/j.jastp.2008.06.014.

Shprits, Y. Y., D. Subbotin, and B. Ni (2009), Evolution of electron fluxes in the outer radiation belt computed with the VERB code, *J. Geophys. Res.*, *114*, A11209, doi:10.1029/2008JA013784.

Sigsbee, K., J. D. Menietti, O. Santolik, and J. B. Blake (2008), Polar PWI and CEPPAD observations of chorus emissions and radiation belt electron acceleration: Four case studies, *J. Atmos. Sol. Terr. Phys.*, *70*, 1774–1788, doi:10.1016/j.jastp.2008.02.005.

Sigsbee, K., J. D. Menietti, O. Santolik, and J. S. Pickett (2010), Locations of chorus emissions observed by the Polar Plasma Wave Instrument, *J. Geophys. Res.*, *115*, A00F12, doi:10.1029/2009JA014579.

Spasojevic, M., and U. S. Inan (2010), Drivers of chorus in the outer dayside magnetosphere, *J. Geophys. Res.*, *115*, A00F09, doi:10.1029/2009JA014452.

Summers, D., C. Ma, N. P. Meredith, R. B. Horne, R. M. Thorne, and R. R. Anderson (2004), Modeling outer-zone relativistic electron response to whistler mode chorus activity during substorms, *J. Atmos. Sol. Terr. Phys.*, *66*, 133–146, doi:10.1016/j.jastp.2003.09.013.

Summers, D. (2005), Quasi-linear diffusion coefficients for field-aligned electromagnetic waves with applications to the magnetosphere, *J. Geophys. Res.*, *110*, A08213, doi:10.1029/2005JA011159.

Summers, D., B. Ni, and N. P. Meredith (2007a), Timescales for radiation belt electron acceleration and loss due to resonant wave-particle interactions: 2. Evaluation for VLF chorus, ELF hiss, and electromagnetic ion cyclotron waves, *J. Geophys. Res.*, *112*, A04207, doi:10.1029/2006JA011993.

Summers, D., B. Ni, and N. P. Meredith (2007b), Timescales for radiation belt electron acceleration and loss due to resonant waveparticle interactions: 1. Theory, *J. Geophys. Res.*, *112*, A04206, doi:10.1029/2006JA011801.

Thorne, R. M., E. J. Smith, R. K. Burton, and R. E. Holzer (1973), Plasmaspheric hiss, *J. Geophys. Res.*, *78*, 1581–1596, doi:10.1029/JA078i010p01581.

Thorne, R. M., T. P. O'Brien, Y. Y. Shprits, D. Summers, and R. B. Horne (2005), Timescale for MeV electron microburst loss during geomagnetic storms, *J. Geophys. Res.*, *110*, A09202, doi:10.1029/2004JA010882.

Tsurutani, B., and E. Smith (1977), Two types of magnetospheric ELF chorus and their substorm dependences, *J. Geophys. Res.*, *82*, 5112–5128, doi:10.1029/JA082i032p05112.

Tsurutani, B. T., O. P. Verkhoglyadova, G. S. Lakhina, and S. Yagitani (2009), Properties of dayside outer zone chorus during HILDCAA events:

Loss of energetic electrons, *J. Geophys. Res.*, *114*, A03207, doi:10.1029/2008JA013353.

Tsyganenko, N. A. (1989), A magnetospheric magnetic field model with a warped tail current sheet, *Planet. Space Sci.*, *37*, 5–20, doi:10.1016/0032-0633(89)90066-4.

Vaivads, A., O. Santolik, G. Stenberg, M. André, C. J. Owen, P. Canu, and M. Dunlop (2007), Source of whistler emissions at the dayside magnetopause, *Geophys. Res. Lett.*, *34*, L09106, doi:10.1029/2006GL029195.

N. L. Bunch and M. Spasojevic, STAR Laboratory, Department of Electrical Engineering, Stanford University, 350 Serra Mall, Stanford, CA 94305, USA. (nbunch@stanford.edu)

Y. Y. Shprits, Institute of Geophysics and Planetary Physics, University of California, Los Angeles, CA 90095-1565, USA.